Small-Angle Neutron Scattering Study of a Cylinder-to-Sphere Order–Order Transition in Block Copolymers

R. Krishnamoorti,* A. S. Silva, and M. A. Modi

Department of Chemical Engineering, University of Houston, Houston, Texas 77204-4792

B. Hammouda

Center for Neutron Research, National Institute of Standards and Technology, Gaithersburg, Maryland 20899

ABSTRACT: The pathway and kinetics of the order–order transition from shear-aligned cylindrical microdomains to spheres arranged on a bcc lattice in a highly asymmetrical block copolymer are monitored using small-angle neutron scattering (SANS). Shear-aligned hexagonally closed-packed cylindrical microdomains were heated to the spherical microdomain region under quiescent conditions, and the microstructure evolution associated with the order–order transition was followed by SANS. The data indicate a rapid decrease in the cylindrical microdomain order and a gradual rise in the signatures associated with the spherical microdomains, thereby suggesting the existence of an intermediate state where the sample is poorly ordered. The duration of this intermediate state increases with increasing distance from the order–order transition and is consistent with previous rheological measurements on unaligned wormlike cylinders. The results of the scattering measurements are compared to the predictions of recent theories describing the cylinder-to-sphere transition.

Introduction

We have recently investigated the pathway and kinetics associated with the cylinder-to-sphere transition in a mixture of a matched diblock and triblock copolymers using linear viscoelastic measurements and ex-situ transmission electron microscopy.[1,2] These measurements suggested that the pathway from unaligned wormlike cylindrically ordered microdomains to a spherically ordered microstate arranged on a bcc lattice is mediated by the presence of a poorly ordered intermediate state exhibiting liquidlike flow characteristics.[1] Further, the structural changes investigated by ex-situ TEM confirm the hypothesis of a poorly ordered intermediate state where the microphase-separated state is poorly defined.[2] The poorly ordered state is, in fact, not unexpected on the basis of the theory presented by Qi and Wang.[3,4] They used a time-dependent Landau–Ginzburg theory to suggest that, during the transition from cylinders to spheres, the order parameter corresponding to the cylindrical state diminishes rapidly while that corresponding to the spherical ordered state grows slowly, indicating an incubation period that resembles a poorly ordered state.

Recent experiments by Ryu et al.[5–7] and Kim et al.,[8,9] on the other hand, indicate that the cylinder-to-sphere transition does in fact occur epitaxially and quite rapidly for the case of shear-aligned cylinders as was observed in earlier studies by Koppi et al.[10] and Sakurai et al.[11] These studies have suggested that the transition is mediated by the presence of undulating cylinders which then lead to an epitaxial growth of bcc spheres. In this paper, we report the pathway and kinetics of the cylinder-to-sphere transition as a function of temperature using small-angle neutron scattering (SANS) on in-situ shear-aligned samples. These measurements pro-

vide a direct method to probe the in-situ temporal evolution of the structural features related to the cylindrical-to-spherical microdomain transition and further provide a direct link to previous experiments on shear-aligned samples.[5–11]

Experimental Section

Detailed characterization information on the material examined is provided in the accompanying paper and in previous publications.[1,2,12] On the basis of previous studies, we assign the order–disorder transition temperature (T_{ODT}) to be 195 ± 5 °C and the cylinder-to-sphere order–order transition temperature (T_{OOT}) to be 138 ± 3 °C. SANS measurements were performed on the 30 m SANS beamline (NG3) at NIST, Gaithersburg, MD. Neutrons with wavelength (λ) of 6 Å and $\Delta\lambda/\lambda$ of 0.15 were used with sample-to-detector distances ranging from 5 to 6.5 m. A 0.5 mm thick sample was loaded in an aluminum shear cell and placed in the in-situ reciprocating shear device developed by Bates and co-workers.[10] The temperature of both sides of the shear cell was independently controlled to within ± 1 °C and had a rapid response insofar as the heating was concerned. The shear device was set on a goniometer stage, allowing for the simultaneous observation of the SANS intensity along two principal directions—with the neutron beam along the velocity gradient direction $(\nabla\mathbf{v})$ and along the neutral direction $(\mathbf{v} \otimes \nabla\mathbf{v})$. For the measurements along the neutral direction, a slit defining an aperture of 10 mm × 0.5 mm was carefully aligned so neutrons would pass through the sample and not scatter from the aluminum cell holders. In some of the measurements reported here (for example, the temperature jump experiments to 150 °C from 130 °C) the slit was used to simultaneously probe the scattering along the two principal directions. Reciprocating steady shear with one of the plates held stationary and the other undergoing a strain amplitude of 100% with a strain rate $|\dot{\gamma}|$ of 5 s^{-1} were performed. Corrections to the SANS data due to the empty cell and background scattering have not been applied.

---

* Corresponding author. E-mail: ramanan@bayou.uh.edu.
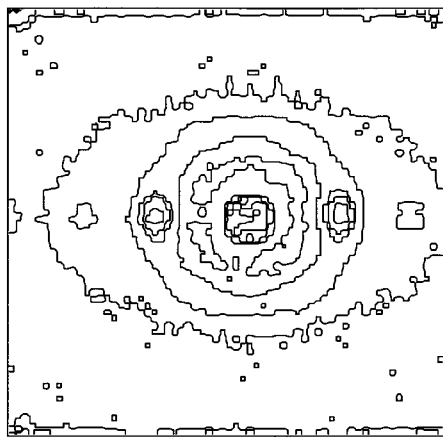
Figure 1. Two-dimensional SANS pattern for a shear-aligned cylindrical sample at 130 °C with neutron beam parallel to the shear gradient direction.
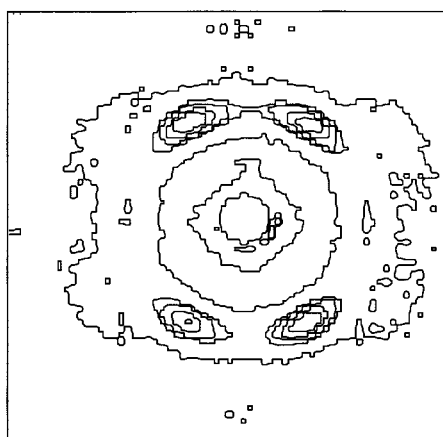
Figure 2. Two-dimensional SANS pattern for a shear-aligned spherical sample at 150 °C with the neutron beam parallel to the shear gradient direction.

Results and Discussion

The two-dimensional scattering pattern from a sample after prolonged large-amplitude reciprocating steady shear at $T = 130$ °C ($T < T_{OOT}$) with the neutron beam parallel to the velocity gradient direction is shown in Figure 1. Two intense spots are observed in the equatorial plane at q^*, with well-developed higher-order scattering peaks observed at $\sqrt{3}q^*$ (Figure 1). Further, when viewed with the neutron beam along the neutral direction, two intense spots on either side of the beam stop, corresponding to the primary peak at q^*, are also observed in the equatorial plane (data not shown). These scattering signatures lead us to conclude that the sample develops well-oriented, hexagonally packed cylinders that are aligned with the cylinder axis along the velocity direction, i.e., parallel orientation.[13] We note that Koppi et al.[10] have shown that, for *perfect* alignment of cylinders along the direction of shear with the neutron beam parallel to the velocity gradient direction, the peak at q^* should be absent and the $\sqrt{3}q^*$ peak should be prominent. However, due to the imperfections of the shear alignment, the q^* peaks are typically observed for parallel aligned cylinders as noted by Koppi et al.[10]

For purposes of comparison, Figure 2 presents the two-dimensional scattering pattern obtained after prolonged large-amplitude reciprocating steady shear for

a sample at 150 °C, i.e., aligned bcc spherical microdomains. The scattering pattern is consistent with that of a twinned bcc structure with higher-order scattering reflections observed at $\sqrt{2}q^*$ and $\sqrt{3}q^*$.[14] Four intense reflections at q^* positioned at 35° to the shear direction are observed, consistent with the degenerate sets of the twinned bcc structure. The higher-order reflections at $\sqrt{2}q^*$ are approximately 55° to the shear direction.

The pathway and kinetics of the cylinder-to-sphere transition were monitored by performing a temperature jump to the spherical state ($T_{OOT} < T < T_{ODT}$, $T = 150$, 160, and 170 °C) on well-aligned cylindrical samples prepared at 130 °C. The temporal evolution of the two-dimensional scattering patterns with the neutron beam parallel to the velocity gradient direction at 150 and 170 °C is shown in Figures 3 and 4, respectively. It has been previously shown that there exists an epitaxial relationship between the ⟨001⟩ axis of the cylinders and the ⟨111⟩ axis of the spheres.[14] The transformation from cylinders to spheres reported here is consistent with that epitaxial relationship, although the pathway is distinctly different at the two temperatures as shown in Figures 3 and 4. In the case of the transformation at 170 °C, it is clear that the initial well-defined spots corresponding to an alignment of the cylinders (both at q^* and $\sqrt{3}q^*$) rapidly disappear within 10 min of heating to the spherical microstate, and the scattering pattern is consistent with that of an unaligned system. Further, the development of the scattering signatures corresponding to the bcc occurs after considerable time following the temperature jump.

The angular dependence of the intensity for the transformation at 150 °C in an annular region centered on the primary peak position q^* is shown in Figure 5a. The corresponding angular dependence of the second-order peak intensities for the same transformation is shown in Figure 5b. The data presented in Figure 5 clearly show that the transformation proceeds via a rapid decrease of the intensities corresponding to the cylindrical structure (also termed as hex) and a slow increase in the intensities corresponding to the bcc structure. These are better illustrated in Figure 6, which displays the temporal evolution of the intensities of the hex and bcc structures at q^* and the higher-order scattering peak. Figure 6 clearly reveals that the intensity of the first- and second-order peaks of the cylindrical microdomains diminish with time, while those corresponding to the first- and second-order peaks of the spherical microdomains gradually increase.

Analogous temporal evolution of the intensities corresponding to the primary peak of the hex and bcc structures for a temperature jump to 170 °C is shown in Figure 7. The intensities corresponding to the peaks of the cylindrical microdomains diminish rapidly as illustrated in the inset of Figure 7. On the other hand, the intensities corresponding to the spherical microdomain structure gradually increase after exhibiting a long incubation period. We note that the same trends were also observed in the development of the second-order scattering peaks for the temperature jump to 170 °C. The slight increase in the intensity corresponding to the hex structures at long times is thought to result from the growth of spherical microdomains that are no longer twinned bcc structures, the usual shear-aligned bcc structure produced. Under quiescent conditions, shear-aligned cubic structures such as spheres arranged on a bcc lattice are known to disorient. Thus, while the
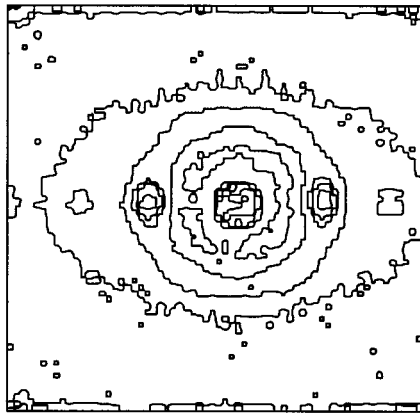
a.

b.

c.

d.

e.
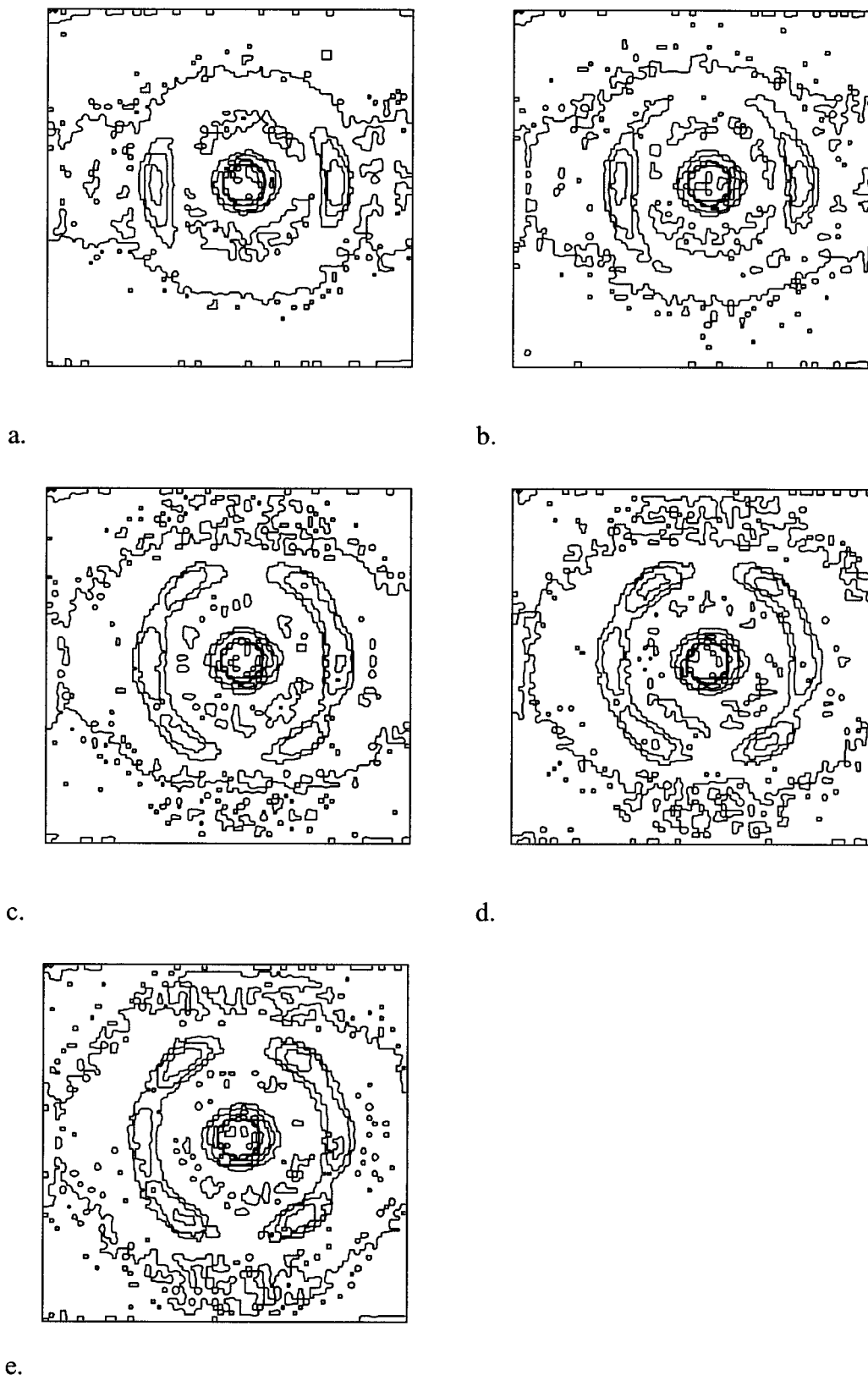
Figure 3. Two-dimensional SANS pattern elucidating the pathway of the cylinder-to-sphere transition for a temperature jump to 150 °C from a well-aligned cylindrical state at 130 °C. The panel (a) corresponds to the well-aligned cylindrical state at time = 0, while panels (b) through (e) are representative patterns after 15, 145, 350, and 560 min, respectively, following the jump to 150 °C.

transformation from shear-aligned cylinders to bcc spheres is undertaken under quiescent conditions, the bcc spheres tend to disorient and may even exhibit some level of biaxial orientation. This disorientation is believed to be the origin of the slight increase in the

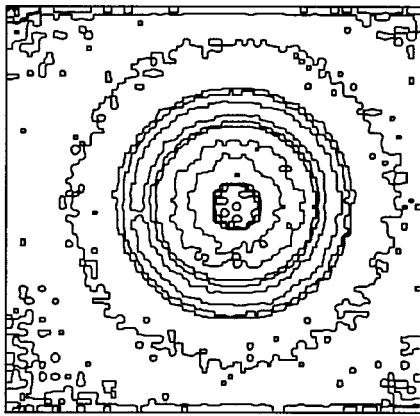equatorial peaks at q^* (the hex signature) at long times in Figure 7.

During the incubation period for the transformation at 170 °C, the intensity at the primary peak position is essentially isotropic, as illustrated by the two-dimen-
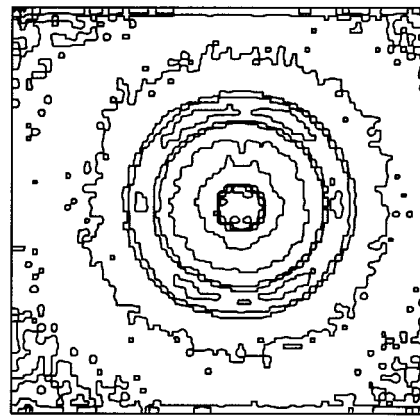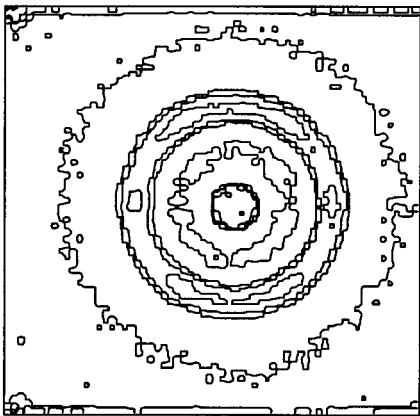
a.
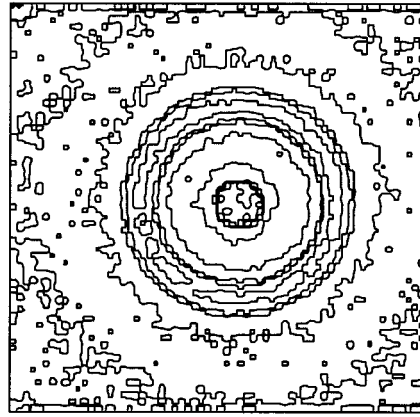
b.

c.

d.

e.

Figure 4. Two-dimensional SANS pattern elucidating the pathway of the cylinder-to-sphere transition for a temperature jump to 170 °C from a well-aligned cylindrical state at 130 °C. The panel (a) corresponds to the well-aligned cylindrical state at time = 0, while panels (b) through (e) are representative patterns after 7, 205, 315, and 415 min, respectively, following the jump to 170 °C.

sional scattering pattern in Figure 4 and by the angular dependence of the intensities in an annular region centered at q^* as shown in Figure 8. This isotropic, or nearly isotropic, behavior persists for about 100 min before the bcc microstructure starts to epitaxially grow. Data similar to that of 170 °C were also obtained for a

temperature jump to 160 °C (not shown) with an incubation time for the bcc microstructure to develop of $\sim$ 40 min.
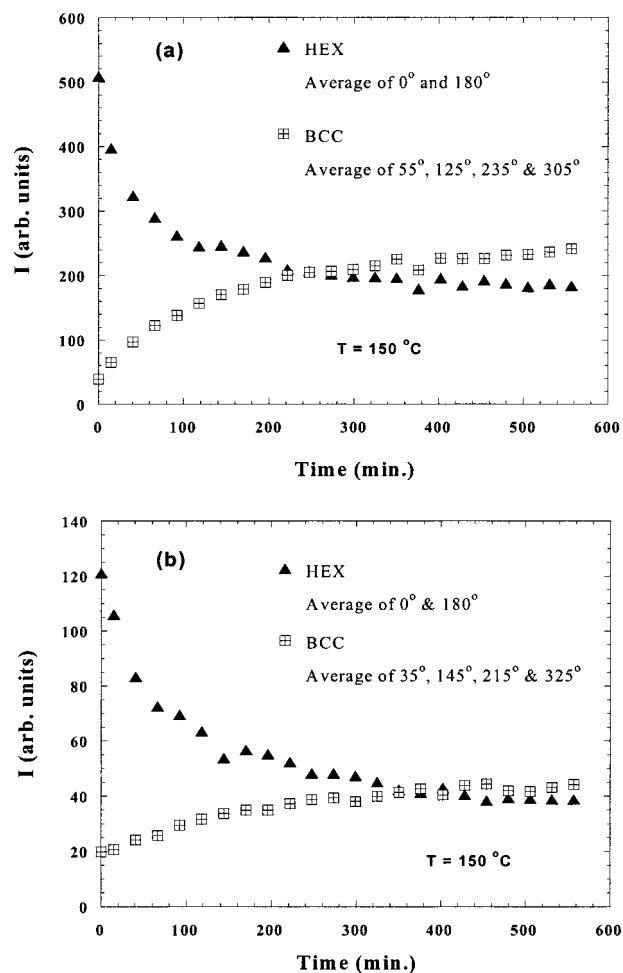
Thus, it appears that the cylinder-to-sphere transition is epitaxial for the case of shear-aligned samples, with the epitaxial relationship being between the $\langle 001 \rangle$ axis
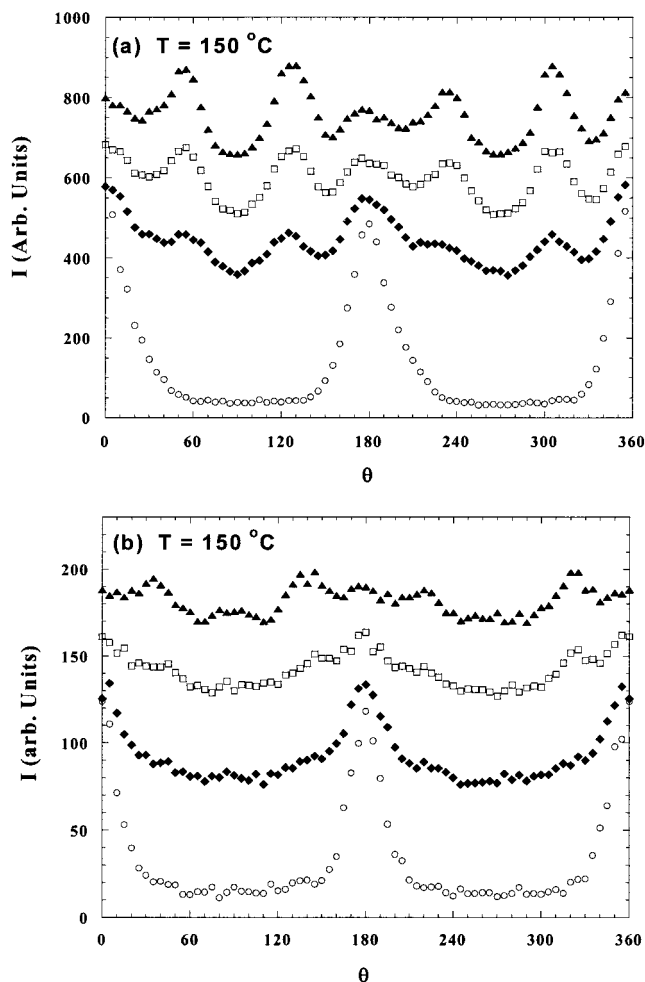
Figure 5. Angular dependence of the SANS intensity in an annular region corresponding to q^* (a) and second-order reflection (b) for the cylinder-to-sphere transition from 130 to 150 °C. The open circles correspond to the initial cylindrical state (i.e., time = 0), while the filled diamonds, open squares, and filled triangles correspond to 90, 220, and 560 min, respectively, after the temperature jump to 150 °C. The second-order reflections (b) are originally located at $\sqrt{3}q^*$ for the cylindrical state and gradually moves to $\sqrt{2}q^*$ for the final spherical state. The data are shifted with respect to each other to avoid overlap.

Figure 6. Time dependence of the SANS intensity at q^* (a) and second-order reflections (b) corresponding to the cylindrical microdomains and spherical microstructure for the temperature jump from 130 to 150 °C. In part (a) the intensity associated with the cylindrical structure was calculated by averaging the intensities at 0° and 180° (i.e., along the equatorial plane in Figure 3). The intensity associated with the spherical microstructure was calculated by averaging the intensities at 55°, 125°, 235°, and 305° (i.e., 35° to the shear direction). In part (b) the intensity associated with the cylindrical structure was calculated by averaging the intensities at 0° and 180° (i.e., along the equatorial plane in Figure 3). The intensity associated with the spherical microstructure was calculated by averaging the intensities at 35°, 145°, 215°, and 325°.

of the cylinders and the $\langle 111 \rangle$ axis of the spheres. The transition between the cylindrical and spherical microdomains is mediated by an intermediate state that exhibits an isotropic scattering pattern (starting from shear-aligned cylinders) with a complete dissolution of the cylindrical structure at higher quench depths, i.e., greater $T - T_{OOT}$. Previously, we had shown that the rheological properties of the intermediate state starting from initial wormlike unaligned cylinders are liquidlike, and this hypothesis was supported by ex-situ electron micrographs of the intermediate states.[2] The length of the initial incubation period, before the signatures of the bcc microstructure are manifested, increases with increasing distance from the OOT: being nearly imperceptible at 150 °C, ~40 min long at 160 °C, and of the order of 100 min at 170 °C. These are consistent with the observations from rheological measurements that the cylinders-to-sphere order–order transition kinetics slow down with increasing distance from the order–order transition.

The SANS data reported here at 150 °C agree qualitatively with the rheological data obtained on a

sample with shear-aligned cylinders quiescently heated to the spherical state ($T = 150$ °C) and shown in the companion paper. However, comparing data for the transition from cylinders to spheres on shear-aligned cylinders (using viscoelasticity and SANS) to that obtained on unaligned wormlike cylinders (using viscoelasticity) clearly reveals that the kinetics are accelerated for the shear-aligned cases (Figure 1 of the preceding paper).

Our results obtained for the temperature jump to 170 °C (and 160 °C) disagree with other experimental studies by Kim et al.[8,9] and Ryu et al.[5-7] They demonstrate that, for polystyrene–polyisoprene diblock and triblock copolymers, the cylindrical microdomain-to-spherical microdomain transition is, in fact, not mediated by a poorly ordered state. The SAXS and TEM data of Ryu et al. clearly indicate that undulating cylinders mediated the cylinder-to-sphere transition in their
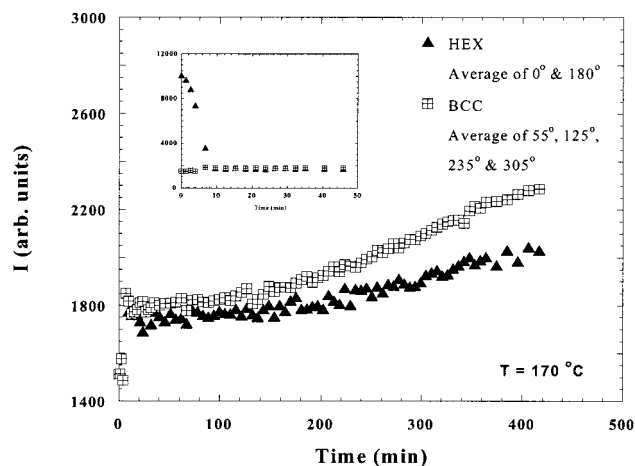
Figure 7. Time dependence of the SANS intensity at q^* corresponding to the cylindrical microdomains and spherical microstructure for the temperature jump from 130 to 170 °C. The intensity associated with the cylindrical structure was calculated by averaging the intensities at 0° and 180° (i.e., along the equatorial plane in Figure 4). The intensity associated with the spherical microstructure was calculated by averaging the intensities at 55°, 125°, 235°, and 305° (i.e., 35° to the shear direction). Shown in the inset are the changes at short times for the scattered intensities of the cylindrical and spherical structures, and the rapidity with which the cylindrical microdomains are dissolved is clearly observed. Note the complete dissolution of the signatures corresponding to the cylindrical microdomains (also see Figure 8) before the gradual growth of the spherical microstructures.
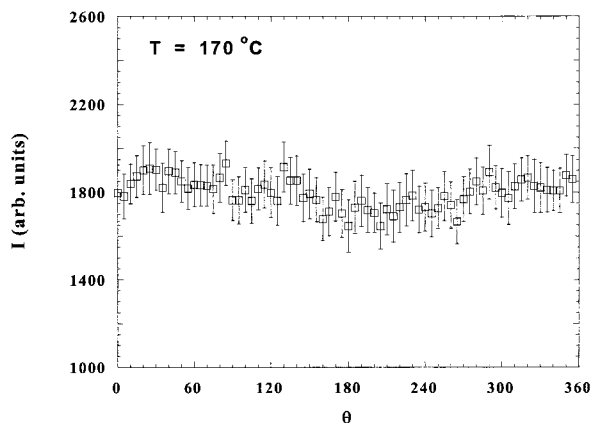
Figure 8. Angular dependence of the SANS intensity in an annular region corresponding to q^* after ~30 min following the jump from 130 to 170 °C. Note that the scattering appears nearly isotropic.

experiments and are consistent with the theoretical results of Qi and Wang[4,5] and Laradji et al.[15]

Kim et al. hypothesize two possible mechanisms for the cylinder-to-sphere transition, i.e., either via the disordered state or via the undulating cylinder structure.[9] They have used a simple free energy calculation to suggest that the transition in their case is mediated by undulating cylinders and not by a disordered liquid-like state. However, in the SAXS data presented by Kim et al., while the higher-order (second and third) small-angle X-ray scattering peaks are observable for the cylindrical and spherical microdomain states, the scattering at intermediate times reveals no higher-order peaks, suggesting the possibility that the transition could be mediated by a poorly ordered state.

One possible suggestion to explain the discrepancy between our results and those previously published

could be the mismatch in the interdomain spacing for the cylindrical and spherical microdomains. Koppi et al.[10] and Sakurai et al.[11] had suggested that the epitaxial behavior of the cylinder-to-sphere transition was a result of the close match of the q^* values across the OOT observed in their case. However, in the measurements by Kim et al.[8,9] and Ryu et al.,[5-7] there is a slight mismatch in the q^* value which results in a reduction in d_{110}^{bcc} as compared to d_{100}^{hex} of less than 10%. Yet, the experimental evidence suggests that the transformation is epitaxial and is mediated by the undulating cylinder state. On the basis of the value of q^* from the SANS data, we estimate d_{100}^{hex} at 130 °C to be 275 ± 5 Å and d_{110}^{bcc} to be 245 ± 5 and 240 ± 5 Å at 150 and 170 °C, respectively. The mismatch in d_{100}^{hex} and d_{110}^{bcc} is somewhat larger than that observed by Kim et al. and Ryu et al. and is a possible source of the differences in structural pathways noted earlier. The mismatch in d_{100}^{hex} and d_{110}^{bcc} increases with increasing $T - T_{OOT}$ and might explain the increased incubation time, where the scattering at the primary peak at q^* remains essentially isotropic, with increasing $T - T_{OOT}$.

Another possibility for the discrepancy is that we are examining a blend of a matched diblock and triblock, which could lead to a smearing of the transition. Ryu et al.[5-7] have addressed this precise issue in their study and have clearly shown that a mixture of matched diblock and triblock behaves *qualitatively* identically to the pure di- and triblock copolymers. Furthermore, systematic studies in our laboratory have suggested that the diblock and triblock copolymers and their mixtures reveal *qualitatively* similar behavior to the data reported in this paper.[16] As expected, the kinetics of the diblock and triblock and their mixtures are quite different.

The differences in the pathway could also be a result of differences in the magnitude of the interaction parameter χ between the copolymer constituents and its temperature dependence. While the product of χN and composition dictates the location of the phase boundaries, it is also possible that, if χ displayed an unusual temperature dependence (i.e., almost independent of temperature or strongly dependent on temperature), it could lead to the observation of different structural pathways for the cylinder-to-sphere transition. The thermodynamic interaction parameter χ, when defined on a consistent volume basis (and we choose 10^{-22} cm^3 for the reference volume[17]), is somewhat larger for the PS−PE$_{62.5}$B$_{37.5}$ case examined here when compared to that of the PS−PI system examined by Kim et al.[8,9] and Ryu et al.[5-7] and the PEP−PEE system studied by Koppi and co-workers.[10]

For PS−PE$_{62.5}$B$_{37.5}$ we estimate, on the basis of the fitting of the SANS data in the disordered state to the random phase approximation, that the temperature dependence of χ (with $v_{ref} = 10^{-22}$ cm^3) can be adequately described by

$$\chi = (0.020 \pm 0.005) + \left(\frac{24 \mp 6}{T}\right) \qquad (1)$$

where T is in kelvin. The estimates of χ for the temperature range of interest are roughly 50% higher than that for PS−PI. However, the temperature dependence of χ indicates the presence of an upper critical solution temperature, and the magnitude of the temperature dependence is comparable to that observed in

other block copolymer systems exhibiting cylinder-to-sphere order−order transitions, i.e., PS−PI and PEP−PEE. Thus, it would appear that the slightly larger interaction parameter, per se, is not responsible for the discrepancy.

On the basis of the experimental results presented in this paper, we surmise the depth of the quench (i.e., $T - T_{OOT}$) to be an important parameter controlling the kinetics and pathway of the order−order transition as noted by the differences in pathways observed at 150 and 170 °C, with a slowing down of the kinetics with increasing $T - T_{OOT}$. The time-dependent Landau−Ginzburg calculation of Qi and Wang[3,4] suggests a rapid decrease of the order parameter followed by a long intermediate period where the order parameter is small and then followed by a gradual increase in the order parameter due to the emergence of the spherical structure from the cylinders. It is also anticipated on the basis of that theory that, for higher quench depths (i.e., for temperatures approaching T_{ODT}), the order parameter in the intermediate time should be weaker. These predictions are consistent with the experimental results reported here for the temperature jumps to 150 and 170 °C, where distinctly different time dependencies of the structural pathways are observed.

Concluding Remarks

The pathway and kinetics of the cylinder-to-sphere transition have been studied using SANS measurements on shear-aligned cylinders. These measurements suggest the possibility of a complete dissolution of the cylindrical structure before the epitaxial growth of the spherical microdomain structure, particularly for large $|T - T_{OOT}|$, and are qualitatively different from the pathway elucidated from previous studies of the cylinder-to-sphere transition on shear aligned samples.[5−11] It is conceivable that the relatively large mismatch in d_{100}^{hex} and d_{110}^{bcc} observed in this study could be responsible for the observed differences in pathways. Further, with increased temperature for the annealing in the spherical state, the mismatch in d_{100}^{hex} and d_{110}^{bcc} increases and is consistent with the observed increase in incubation time with increased annealing temperature. The pathway suggested for the shear-aligned samples using SANS are qualitatively similar to the one hypothesized by us based on linear viscoelastic and transmission electron microscopy on unoriented wormlike cylinders transforming to bcc spheres. The kinetics however are dramatically hastened for the case of shear-aligned samples as compared to the unaligned cylinders.

References and Notes

(1) Modi, M. A.; Krishnamoorti, R.; Tse, M. F.; Wang, H.-C. *Macromolecules* **1999**, *32*, 4088.
(2) Krishnamoorti, R.; Modi, M. A.; Tse, M. F.; Wang, H.-C. *Macromolecules* **2000**, *33*, 3810.
(3) Qi, S.; Wang, Z.-G. *Phys. Rev. Lett.* **1996**, *76*, 1679.
(4) Qi, S.; Wang, Z.-G. *Phys. Rev. E* **1997**, *55*, 1682.
(5) Ryu, C. Y.; Lee, M. S.; Hajduk, D. A.; Lodge, T. P. *J. Polym. Sci., Part B: Polym. Phys.* **1997**, *35*, 2811.
(6) Ryu, C. Y.; Vigild, M. E.; Lodge, T. P. *Phys. Rev. Lett.* **1998**, *81*, 5354.
(7) Ryu, C. Y.; Lodge, T. P. *Macromolecules* **1999**, *32*, 7190.
(8) Kim, J. K.; Lee, H. H.; Gu, Q.-J.; Chang, T.; Jeong, Y. H. *Macromolecules* **1998**, *31*, 4045.
(9) Kim, J. K.; Lee, H. H.; Ree, M.; Lee, K.-B.; Park, Y. *Macromol. Chem. Phys.* **1998**, *199*, 641.
(10) Koppi, K. A.; Tirrell, M.; Bates, F. S.; Almdal, K.; Mortensen, K. *J. Rheol.* **1994**, *38*, 999.
(11) Sakurai, S.; Hashimoto, T. *Macromolecules* **1996**, *29*, 740. Sakurai, S.; Umeda, H.; Taie, K.; Nomura, S. *J. Chem. Phys.* **1996**, *105*, 8902. Sakurai, S.; Kawada, H.; Hashimoto, T.; Fetters, L. *Macromolecules* **1993**, *26*, 5796. Sakurai, S.; Hashimoto, T.; Fetters, L. *J. Polym. Prepr., Jpn., Soc. Polym. Sci., Jpn.* **1991**, *40*, 770.
(12) Tse, M. F.; Wang, H.-C.; Shaffer, T. D.; McElrath, M. C.; Modi, M.; Krishnamoorti, R. Presented at the 152nd Meeting of Rubber Division, American Chemical Society, Cleveland, Oct 21−24, 1997; paper no. 17.
(13) Bates, F. S.; Koppi, K. A.; Tirrell, M.; Almdal, K.; Mortensen, K. *Macromolecules* **1994**, *27*, 5934. Schulz, M. F.; Bates, F. S.; Almdal, K.; Mortensen, K. *Phys. Rev. Lett.* **1994**, *73*, 86.
(14) Almdal, K.; Koppi, K. A.; Bates, F. S. *Macromolecules* **1993**, *26*, 4058.
(15) Laradji, M.; Shi, A. C.; Desai, R. C.; Noolandi, J. *Phys. Rev. Lett.* **1997**, *78*, 2577. Laradji, M.; Shi, A. C.; Noolandi, J.; Desai, R. C. *Macromolecules* **1997**, *30*, 3242.
(16) Modi, M. A.; Krishnamoorti, R. Unpublished data.
(17) Bates, F. S.; Schulz, M. F.; Rosedale, J. H.; Almdal, K. *Macromolecules* **1992**, *25*, 5547.
(18) Certain equipment and instruments or materials are identified in this paper in order to adequately specify the experimental details. Such identification does not imply recommendation by the National Institute of Standards and Technology, nor does it imply the materials are necessarily the best available for the purpose.

MA991842P